HHS Public Access

Author manuscript

Mol Imaging Biol. Author manuscript; available in PMC 2018 April 01.

Published in final edited form as:

Mol Imaging Biol. 2017 April ; 19(2): 225–232. doi:10.1007/s11307-016-0995-0.

Creatine CEST MRI for Differentiating Gliomas with Different Degrees of Aggressiveness

Kejia Cai[1,2], **Rong-Wen Tain**[1], **Xiaohong Joe Zhou**[1,2], **Frederick C. Damen**[1], **Alessandro M. Scotti**[1,2], **Hari Hariharan**[3], **Harish Poptani**[4], and **Ravinder Reddy**[3]

[1]Department of Radiology and the Center for MR Research, College of Medicine, University of Illinois at Chicago, Chicago, IL, USA

[2]Department of Bioengineering, University of Illinois at Chicago, Chicago, IL, USA

[3]The Center for Magnetic Resonance and Optical Imaging, Department of Radiology, School of Medicine, University of Pennsylvania, Philadelphia, PA, USA

[4]Centre for Preclinical Imaging, University of Liverpool, Liverpool, UK

Abstract

Purpose—Creatine (Cr) is a major metabolite in the bioenergetic system. Measurement of Cr using conventional MR spectroscopy (MRS) suffers from low spatial resolution and relatively long acquisition times. Creatine chemical exchange saturation transfer (CrCEST) magnetic resonance imaging (MRI) is an emerging molecular imaging method for tissue Cr measurements. Our previous study showed that the CrCEST contrast, obtained through multicomponent Z-spectral fitting, was lower in tumors compared to normal brain, which further reduced with tumor progression. The current study was aimed to investigate if CrCEST MRI can also be useful for differentiating gliomas with different degrees of aggressiveness.

Procedures—Intracranial 9L gliosarcoma and F98 glioma bearing rats with matched tumor size were scanned with a 9.4 T MRI scanner at two time points. CEST Z-spectra were collected using a customized sequence with a frequency-selective rectangular saturation pulse (B_1 = 50 Hz, duration = 3 s) followed by a single-shot readout. Z spectral data were fitted pixel-wise with five Lorentzian functions, and maps of CrCEST peak amplitude, linewidth, and integral were produced. For comparison, single-voxel proton MR spectroscopy (^{1}H-MRS) was performed to quantify and compare the total Cr concentration in the tumor.

Results—CrCEST contrasts decreased with tumor progression from weeks 3 to 4 in both 9L and F98 phenotypes. More importantly, F98 tumors had significantly lower CrCEST integral compared to 9L tumors. On the other hand, integrals of other Z-spectral components were unable to differentiate both tumor progression and phenotype with limited sample size.

Correspondence to: Kejia Cai; kcai@uic.edu.

Compliance with Ethical Standards

Conflict of Interest

The authors declare that they have no conflict of interest.

Conclusions—Given that F98 is a more aggressive tumor than 9L, this study suggests that CrCEST MRI may help differentiate gliomas with different aggressiveness.

Keywords

Creatine; CEST; Glioma; Aggressiveness

Introduction

Brain tumors are the leading cause of cancer death among children and young adults in the USA [1, 2]. About 80 % of malignant brain tumors are of glial origin and are generally referred to as gliomas. Although the prognosis for patients with high-grade gliomas is generally poor, the choice of treatment strategy can have a significant impact on survival. Tumor grade or the degree of malignancy is one of the key factors in determining the optimal treatment paradigm. Although histological grading is the gold standard, it suffers from sampling error and the inability to evaluate residual tumor tissue after cytoreductive surgery. Methods for examining spatial heterogeneity are particularly important for gliomas because the lesions may be composed of regions with different malignancies [3]. Among these methods, magnetic resonance imaging (MRI) parameters have shown correlations with clinical outcome, hence contribute to individualized treatment planning [4, 5]. Although conventional MRI (T_1, T_2, and contrast enhanced MRI) is a useful clinical tool for identifying soft-tissue contrast and morphological changes in patients with gliomas, it is not very accurate in terms of imaging-based tumor grading [3, 6–9]. Therefore, alternative MRI methods based on noninvasive and endogenous contrasts are desirable to probe tumor metabolism, determine tumor grade, and to guide treatment planning.

Chemical exchange saturation transfer (CEST) MRI is an emerging molecular imaging technique that detects metabolites based on proton-exchange properties [10, 11]. CEST measures the reduction of bulk water magnetization due to the exchange of selectively saturated protons between the solute metabolites and water [12–16]. The prolonged saturation transfer process in CEST experiments leads to an enhancement in the detection sensitivity compared to the direct measurement by MR spectroscopy (MRS) [17, 18]. CEST MRI sequences typically consist of a long pre-saturation pulse or a pulse train followed by a readout. CEST effect from amine, amide, and hydroxyl exchangeable protons has been demonstrated to provide spatial maps of those metabolites in the tissue noninvasively. CEST MRI has been previously used to detect amide protons (amide proton transfer or amide proton transfer (APT)) associated with peptides and proteins [19], liver glycogen [20], cartilage glycosaminoglycans [21], and glucose [22] with high spatial resolution at the millimeter or sub-millimeter level. Recently, CEST MRI was demonstrated for molecular imaging of metabolites, including glutamate [17, 23–25], myo-inositol (MI) [26, 27], and creatine (Cr) [28–31], that are typically observed in brain using MRS.

Creatine, phosphocreatine (PCr), and adenosine-5-triphosphate (ATP) are major metabolites of the enzyme creatine kinase (CK), an important enzyme in the bioenergetic system that catalyzes the reversible conversion of Cr into PCr by utilizing ATP [3, 32, 33]. PCr provides phosphate to produce ATP when it is converted to Cr. In 1939, Belitzer and Tsybakova

demonstrated that oxygen consumption increases strongly in the presence of Cr [34], whose concentration was recognized as an important kinetic parameter in the regulation of respiration and energy fluxes. Although MRS can measure Cr signals, it suffers from low spatial resolution and long acquisition times [35, 36]. Recently, CEST MRI has been used to study creatine (CrCEST) and other metabolites in CK, including PCr, ATP, and adenosine diphosphate (ADP) [18]. Under physiological conditions, CEST contrast from those compounds is observed predominantly from Cr with negligible contributions from PCr, ADP, or ATP. It has been shown that CrCEST MRI has over 1000 times higher detection sensitivity compared to single-voxel proton MRS (^{1}H-MRS) [18], enabling high-resolution mapping of Cr signal within the tissue.

The CrCEST technique has been demonstrated in infarcted hearts [29], muscles [30, 31], and brain tumors [28]. As an example, we have earlier demonstrated that CrCEST can measure Cr changes in muscle following plantar flexion exercise [30, 31], showing good agreement with the recovery kinetics measured using ^{31}P-MRS. In addition, our recent study on a rat model of 9L gliosarcomas demonstrated spatial mapping of Cr distributions in tumor-bearing brain [28] using CrCEST contrast obtained through multicomponent fitting of CEST Z-spectra. The fitted CrCEST integrals, the area under the CrCEST peak, decreased in tumors compared to normal brain tissues and reduced further with tumor progression, in conjunction to previous studies [37–39].

The purpose of the present study is to investigate whether CrCEST MRI can be useful in differentiating gliomas (e.g., 9L and F98 xenografts) with different degrees of aggressiveness. F98 glioma is more aggressive than 9L gliosarcoma, with regard to pre-existing vessels [40], cellular infiltration [41], immunogenesis, growth pattern, lethality [42], and prognosis from therapies [43]. In this study, 9L and F98 intracranially transplanted rat models were scanned with MRI and the CrCEST contrasts between the two models were compared. Tumor ^{1}H-MRS results were used to compare with the CrCEST findings.

Materials and Methods

All animal experiments were performed according to protocols approved by the Institutional Animal Care and Use Committee (IACUC) at the University of Pennsylvania, USA. Tumor cells (9L gliosarcoma and the more aggressive F98 glioma) were implanted into the brains of Fisher rats using well-established methods [17, 44]. Tumor-bearing rats (n = 5 for 9L or F98 glioma) received MRI scans longitudinally at weeks 3 and 4 post-tumor implantation. The imaging studies were performed at a 9.4 T Varian horizontal MRI scanner for small animals with a 35-mm commercial rat head coil (M2M Imaging, Cleveland, OH). Note that one rat from each group could not survive for the week 4 scans. For MRI, initial multislice T_2-weighted anatomical images (TR/TE = 2/0.04 s, ten slices with 2 mm thickness) were used for tumor localization. Tumor volumes were estimated from those anatomical images as one half $\alpha \times \beta^2$, where α and β are the long and short axes of tumor, respectively.

CEST MRI and Z-Spectral Fitting

Z-spectra were acquired from the tumor central slice with a 50 Hz or 1.2 μT squared saturation pulses with a total duration of 3 s. A single-shot fast low-angle shot imaging

(FLASH) readout [17] was used for centric K-space acquisition. As described in a previous study [28], the details of the readout include shot TR = 11.4 s, readout TR/TE = 6/3 ms, field of view = 30 × 30 mm^2, matrix size = 128 × 128, 2 mm slice thickness, and 2 averages. The whole Z-spectrum took ~24 min to acquire and consisted of 61 saturation offsets: ±100, ±50, ±25, ±12 to ± 6 ppm with 1 ppm step size, and ± 5 to 0 ppm with 0.25 ppm step size. B_0 and B_1 maps were acquired according to previous studies [17]. In brief, B_0 maps were constructed from the ratio of Δphase/ΔTE when TE varied (3.0, 3.5, and 4.0 ms). The relative B_1 maps, on the other hand, were produced from two images acquired at different flip angels (30° and 60°) using a flip-crush sequence (readout TR/TE = 6/3 ms, shot TR = 9 s, and matrix size = 128 × 128).

Z-spectra (from −12 to +12 ppm) were center-corrected with B_0 map and fitted with a sum of five Lorentzian functions corresponding to five main physicochemical processes expressed in the spectrum: Nuclear Overhauser Enhancement (NOE), semi-solid magnetization transfer contrast (MTC), direct saturation of bulk water, the CrCEST, and the amide proton transfer (APT). These effects and the corresponding fittings were centered at −3.2, −1.5, 0, 2.0 and 3.6 ppm, respectively. The nonlinear fitting was performed in MATLAB 7. 0 (Natick, MA, USA), as described in a previous study [28].

MR Spectroscopy

Following localized shimming at the voxels of interest (voxel size = 3 × 1.5 × 2 mm^3) and water suppression with variable pulse power and optimized relaxation delays (VAPOR) [45], ^{1}H-MRS was obtained from the tumor and the contralateral healthy thalamic region, respectively, using a point-resolved spectroscopy (PRESS) [46] sequence and TR/TE = 3000/13 ms. Each water-suppressed spectrum (256 averages) took about 13 min. The corresponding water reference spectra were acquired with 32 averages which took ~1.5 min.

As described in a previous study [28], both water-suppressed and water reference spectra were fitted using a time domain fitting program MRUI [47, 48] and its method called advanced method for accurate, robust and efficient spectral fitting (AMARES). In brief, spectra were apodized with a 20 Hz Gaussian function, phase corrected, and fitted with Lorentzian functions. For quantification of total Cr concentration, the fitted integral of total Cr peak (at ~3 ppm) was normalized to the water reference integral.

Statistical Analysis

The voxel-wise fitted peak amplitude, linewidth, and integral were averaged within ROIs of tumors defined by anatomical images. Assuming normal distributions, those values were compared between different types of tumors with unpaired one-tailed Student's *t* tests. Paired one-tailed Student's *t* test was used to compare these parameters obtained at different time points. The difference was considered to be significant if $p < 0.05$. Values are reported as mean ± standard error (SE).

Results

From week 3 to week 4, tumor volumes grew from 21.3 ± 2.7 to 151.1 ± 29.5 mm^3 for the 9L and 16.8 ± 4.3 to 138.0 ± 17.7 mm^3 for the F98 tumors. Note that at each time point,

there was no statistical difference ($p > 0.05$) in tumor volume between the two types of tumors. As demonstrated in Fig. 1a, b, Z-spectra fitting allowed for quantification of CrCEST from other concomitant effects, including the intrinsic MTC asymmetry [49], the aliphatic NOE effect [50], and other major CEST effect from APT [51]. The corresponding B_0 map (Fig. 1c) was used for the center correction of Z-spectra. Figure 1d shows a representative relative B_1 map of the brain with mean ± standard deviation of 1.000 ± 0.011. Given that B_1 maps were consistently found to be homogenous across the brain, B_1 correction of Z-spectra or CEST contrasts was not performed in this study. If needed, B_1 correction of CEST maps and hence Z-spectra may be performed according to our previously published calibration-based method [52].

CrCEST quantified with Z-spectra fitting produced three major contrast parameters including the amplitude, the linewidth, and the integral of the CrCEST peak. The contrasts in 9L and F98 tumors were compared at two imaging time points (Fig. 2). Despite the 7–8 times growth in tumor volume from week 3 to week 4, CrCEST amplitude of each tumor type remained similar with tumor progression (9.8 ± 0.8 to 10.0 ± 0.7 % in 9L, $p = 0.10$ and 7.9 ± 0.3 to 8.2 ± 0.2 % in F98, $p = 0.35$). When data from both time points was summed, significantly lower CrCEST amplitude was observed in F98 tumors compared to 9L tumors (9.9 ± 0.5 % in 9L vs 8.1 ± 0.2 % in F98, $p < 0.005$; Fig. 2a). On the other hand, CrCEST linewidth was not significantly different between the two tumor types (2.0 ± 0.1 ppm in 9L vs 1.8 ± 0.1 ppm in F98, $p = 0.16$) but reduced significantly from week 3 to week 4 in each tumor model (Fig. 2b; 2.1 ± 0.2 to 1.8 ± 0.1 ppm in 9L with $p < 0.05$; 1.9 ± 0.0 to 1.7 ± 0.1 ppm in F98 with $p < 0.05$). Interestingly, CrCEST integral proved to be able to differentiate both the tumor progressions from week 3 to week 4 (32.5 ± 4.7 to 28.5 ± 3.4 ppm% in 9L with $p < 0.05$; 23.9 ± 1.2 to 22.0 ± 0.7 ppm% in F98 with $p < 0.05$) and the tumor phenotypes between 9L and F98 (Fig. 2c; 30.7 ± 3.1 ppm% in 9L vs 23.1 ± 0.8 ppm% in F98, $p < 0.05$). On the other hand, despite that APT integral can differentiate tumor progression from week 3 to week 4 (Fig. 3a; 13.7 ± 0.6 to 17.8 ± 1.0 ppm% in 9L with $p < 0.05$; 12.6 ± 1.1 to 17.3 ± 1.0 ppm% in F98 with $p < 0.05$) and MTC integral can differentiate tumor types (Fig. 3c; 572.6 ± 9.6 ppm% in 9L vs 613.0 ± 16.8 ppm% in F98 combining weeks 3 and 4, $p < 0.05$), none of the fitted integrals of APT, NOE, and MTC were able to differentiate both tumor progression and phenotype (Fig. 3). Representative CrCEST, APT, NOE, and MTC integral maps are shown in Fig. 4. Fitting correlation coefficient R^2 maps in Fig. 4 demonstrated good fitting performance (R^2 close to 1) in the majority of brain regions except for cerebrospinal fluid (CSF), where the metabolite concentrations are much lower.

As shown in ^{1}H-MRS spectra (Fig. 5), the total Cr signals appeared to reduce with tumor progression in both types of tumors (6.3 ± 1.0 to 4.2 ± 0.3 mM in 9L, $p = 0.12$; 7.7 ± 1.5 to 5.3 ± 1.0 mM in F98, $p = 0.16$). However, such reduction was not statistically significant ($p < 0.05$; Fig. 4b). Moreover, no significant difference was seen in ^{1}H-MRS between 9L and F98 tumors (5.4 ± 0.6 mM in 9L vs 6.3 ± 0.9 mM in F98, $p = 0.20$).

Discussion

CEST contrast at a specific frequency offset is typically quantified based on the MT ratio asymmetry by subtracting two off-resonance Z-spectral signals with equal separation from the water resonance. Such quantification reduces the contamination from the direct water saturation and MTC. However, this approach cannot remove contamination arising from the intrinsic MTC asymmetry [49], the aliphatic NOE effect [50], and other major CEST effects such as those from APT [51]. Hence, an alternative quantification method based on Z-spectral fitting with multicomponents [28] was used to minimize these potential confounding factors.

Our previous study [28] (in its Table 1) demonstrated that the alternative multicomponent Z-spectra fitting method produces parameters that are consistent with the values found in the literature. For example, we observed decreased MTC [53, 54], higher water content [55], and higher APT [19] in tumors compared to normal brain tissues. We also observed a negative offset of semi-solid MTC located at around −2 ppm from water [49]. The fitted MTC linewidth is reasonably large (over 20 ppm) due to the extremely short bound water T_2 [49].

Through the Z-spectral fitting, CrCEST amplitude, linewidth, and integral were obtained. Under fixed saturation parameters, the CEST amplitude is related to metabolite concentration, proton exchange rate (pH related), and tissue T_1 [28, 56]. With a limited sample size in this study, although CrCEST amplitude differentiated tumor phenotypes, it had limited utility for detection of tumor progression. The linewidth of a CEST peak, on the other hand, is dependent on a different set of factors, including T_2 of exchangeable protons, static field inhomogeneity, proton exchange rate, tissue T_1, and saturation amplitude B_1 [28]. CrCEST linewidth could differentiate the tumor progression but was not able to separate two tumor phenotypes. CrCEST integral intrinsically combines the information of both the amplitude and the linewidth, leading to a higher sensitivity that allows the differentiation of both phenotypes as well as tumor progression. On the other hand, the fitted APT, NOE, and MTC integrals failed to differentiate both tumor phenotypes and progression under the condition of limited sample size.

Our CrCEST results indicate that Cr reduces as tumor progresses with increasing aggressiveness. Given that the creatine–CK system is likely related to tumor bioenergetics and metabolism through regulation of ATP production, the relationship between creatine–CK system and cancer malignancy has been a focal point of investigation [57]. Our imaging observations on CrCEST agree with published studies that show decreased level of Cr and CK activity in several different types of cancer [58–61]. Particularly, Patra *et al.* found that the Cr content and CK activity both progressively decreased in muscle upon transformation to sarcoma and with increased malignancy [57, 62]. However, there are also reports demonstrating increased CK in some tumor tissues [63, 64]. Cr reduction in tumor could be a more complicated process than a consequence solely due to the elevation of tumor bioenergetics or metabolism. Tissue cell type and cellular composition may both affect the Cr level.

In our study, ^{1}H-MRS of total Cr from the tumors demonstrated a trend of Cr reduction with tumor progression. However, it had limited power for the differentiation of tumor types under the condition of limited sample size. In fact, the Cr concentration quantified from ^{1}H-MRS (Fig. 5b) distributed among the four study groups (two tumor types and two time points) with a different pattern from CrCEST integrals (Fig. 2c). This maybe because ^{1}H-MRS quantifies the total Cr (Cr + PCr) due to the overlap of Cr and PCr, while CrCEST quantifies only Cr with negligible contribution from PCr [18, 65]. In addition, ^{1}H-MRS and CrCEST MRI may have different sensitivity and specificity in the detection of tissue Cr.

The detection specificity of CrCEST for tissue Cr may remain a concern. In the previous work, the CEST peak at ~2 ppm was tentatively assigned to glutamine and protein [66]. However, it has been recently proven that CEST effect from glutamine's fast-exchanging amine protons cannot be detected under physiological and pathological pHs [12, 17]. Recently, researchers intended to assign CEST at +2 ppm to amine protons in general [67, 68]. Particularly, Jin *et al.* suggested the contribution from Cr amine protons [67]. However, no studies have quantitatively investigated this assignment. Among the major brain and brain tumor metabolites with slow to intermediate exchangeable protons, only Cr amine or guanidinium protons exhibit CEST effect centered at +2 ppm from water [18, 69]. Therefore, suggest that Cr is a major contributor to the CEST peak at 2 ppm, which is consistent with earlier studies [70, 71]. For example, Arus *et al.* assigned the observed 6.7 ppm (or +2 ppm from water resonance) peak in intact muscle MR spectrum to Cr [70]. A recently published paper on CrCEST and its application in myocardial infarct also demonstrated that the 2 ppm peak is mainly due to Cr [29]. However, potential contributions from other CEST-expressing metabolites, such as glutamate, glucose, proteins, peptides, and changes in pH and relaxation times, cannot be ruled out.

The limitations of this study include limited sample size and the use of only two tumor phenotypes. Although the statistical tests favored CrCEST for the differentiation of glioma aggressiveness, one could not underestimate the values of other imaging and spectroscopic parameters, such as APT, NOE, MTC, and metabolite concentrations from ^{1}H-MRS, for the same purpose. With a larger sample size, these parameters may also be used to differentiate tumor aggressiveness based on their respective physiological aspects. It is also a limitation of this study that we did not acquire data for mapping relaxation times given that tissue relaxations (T_1, T_2, and T_2*) may affect the Z-spectral analysis. For example, the linewidth of a CEST peak may be affected by T_2 relaxation time [28] and the CEST amplitude may be affected by T_1 relaxation time [56]. A thorough discussion on how relaxation times influence the Z-spectral analysis requires a separated study in the future.

Nevertheless, we have demonstrated that CrCEST MRI can be valuable in differentiation of tumor aggressiveness. In addition to relaxation-based MRI [72, 73], contrast-enhanced MRI [74, 75], perfusion MRI [76, 77], and MRS [78, 79] that were used for glioma grading [80], endogenous CrCEST can be another contender for improving tumor characterization with its metabolic and possibly bioenergetic information.

Conclusion

In this preliminary study, we demonstrate that CrCEST contrasts reduce with glioma progression and aggressiveness. Although tissue cell type and cellular composition in the tumor may partially explain such reduction, CrCEST MRI of tumor bioenergetics may help to differentiate the aggressiveness of glioma.

Acknowledgments

We gratefully acknowledge the discussions with Drs. Mohammad Haris and Anup Singh from the Center for MR and Optical Imaging at University of Pennsylvania. Our sincere thanks are also due to Drs. Weixia Liu and Stephen Pickup for their imaging assistance as well as Ranjit Ittyerah and Dr. Damodar Reddy for their help with the animal model. This work was partially supported by the National Center for Research Resources and the National Institute of Biomedical Imaging and Bioengineering of the National Institutes of Health through grant number P41 EB015893 and the Department of Radiology and the Center for Magnetic Resonance Research at University of Illinois at Chicago.

References

1. Bleyer WA. Epidemiologic impact of children with brain tumors. Childs Nerv Syst. 1999; 15:758–763. [PubMed: 10603019]
2. Panigrahy A, Bluml S. Neuroimaging of pediatric brain tumors: from basic to advanced magnetic resonance imaging (MRI). J Child Neurol. 2009; 24:1343–1365. [PubMed: 19841424]
3. Allison GT, Fujiwara T. The relationship between EMG median frequency and low frequency band amplitude changes at different levels of muscle capacity. Clin Biomech. 2002; 17:464–469.
4. Lin A, Bluml S, Mamelak AN. Efficacy of proton magnetic resonance spectroscopy in clinical decision making for patients with suspected malignant brain tumors. J Neurooncol. 1999; 45:69–81. [PubMed: 10728912]
5. Wong ET, Jackson EF, Hess KR, et al. Correlation between dynamic MRI and outcome in patients with malignant gliomas. Neurology. 1998; 50:777–781. [PubMed: 9521274]
6. Dean BL, Drayer BP, Bird CR, et al. Gliomas: classification with MR imaging. Radiology. 1990; 174:411–415. [PubMed: 2153310]
7. Watanabe M, Tanaka R, Takeda N. Magnetic resonance imaging and histopathology of cerebral gliomas. Neuroradiology. 1992; 34:463–469. [PubMed: 1436452]
8. Kondziolka D, Lunsford LD, Martinez AJ. Unreliability of contemporary neurodiagnostic imaging in evaluating suspected adult supratentorial (low-grade) astrocytoma. J Neurosurg. 1993; 79:533–536. [PubMed: 8410222]
9. Ginsberg LE, Fuller GN, Hashmi M, et al. The significance of lack of MR contrast enhancement of supratentorial brain tumors in adults: histopathological evaluation of a series. Surg Neurol. 1998; 49:436–440. [PubMed: 9537664]
10. Forsen S, Hoffman R. Study of moderately rapid chemical exchange reactions by means of nuclear magnetic double resonance. J Chem Phys. 1963; 39:2892–2901.
11. Wolff S, Balaban R. NMR imaging of labile proton-exchange. J Magn Reson. 1990; 86:164–169.
12. Ward KM, Aletras AH, Balaban RS. A new class of contrast agents for MRI based on proton chemical exchange dependent saturation transfer (CEST). J Magn Reson. 2000; 143:79–87. [PubMed: 10698648]
13. Sherry AD, Woods M. Chemical exchange saturation transfer contrast agents for magnetic resonance imaging. Ann Rev Biomed Eng. 2008; 10:391–411. [PubMed: 18647117]
14. Zhou J, van Zijl PC. Chemical exchange saturation transfer imaging and spectroscopy. Prog Nucl Magn Reson Spectrosc. 2006; 48:109–136.
15. van Zijl PC, Yadav NN. Chemical exchange saturation transfer (CEST): what is in a name and what isn't? Magn Reson Med. 2011; 65:927–948. [PubMed: 21337419]

16. Kogan F, Hariharan H, Reddy R. Chemical Exchange Saturation Transfer (CEST) imaging: description of technique and potential clinical applications. Curr Radiol Rep. 2013; 1:102–114. [PubMed: 23730540]
17. Cai K, Haris M, Singh A, et al. Magnetic resonance imaging of glutamate. Nat Med. 2012; 18:302–306. [PubMed: 22270722]
18. Haris M, Nanga RP, Singh A, et al. Exchange rates of creatine kinase metabolites: feasibility of imaging creatine by chemical exchange saturation transfer MRI. NMR Biomed. 2012; 25:1305–1309. [PubMed: 22431193]
19. Zhou J, Lal B, Wilson DA, et al. Amide proton transfer (APT) contrast for imaging of brain tumors. Magn Reson Med. 2003; 50:1120–1126. [PubMed: 14648559]
20. van Zijl PC, Jones CK, Ren J, et al. MRI detection of glycogen in vivo by using chemical exchange saturation transfer imaging (glycoCEST). Proc Natl Acad Sci U S A. 2007; 104:4359–4364. [PubMed: 17360529]
21. Ling W, Regatte RR, Navon G, et al. Assessment of glycosaminoglycan concentration in vivo by chemical exchange-dependent saturation transfer (gagCEST). Proc Natl Acad Sci U S A. 2008; 105:2266–2270. [PubMed: 18268341]
22. Walker-Samuel S, Ramasawmy R, Torrealdea F, et al. In vivo imaging of glucose uptake and metabolism in tumors. Nat Med. 2013; 19:1067–1072. [PubMed: 23832090]
23. Cai K, Singh A, Roalf DR, et al. Mapping glutamate in subcortical brain structures using high-resolution GluCEST MRI. NMR Biomed. 2013; 26:1278–1284. [PubMed: 23553932]
24. Haris M, Nath K, Cai K, et al. Imaging of glutamate neurotransmitter alterations in Alzheimer's disease. NMR Biomed. 2013; 26:386–391. [PubMed: 23045158]
25. Haris M, Singh A, Cai K, et al. High resolution mapping of modafinil induced changes in glutamate level in rat brain. PLoS One. 2014; 9:e103154. [PubMed: 25068408]
26. Haris M, Cai K, Singh A, et al. In vivo mapping of brain myoinositol. Neuroimage. 2011; 54:2079–2085. [PubMed: 20951217]
27. Haris M, Singh A, Cai K, et al. MICEST: a potential tool for noninvasive detection of molecular changes in Alzheimer's disease. J Neurosci Methods. 2013; 12:87–93.
28. Cai K, Singh A, Poptani H, et al. CEST signal at 2ppm (CEST@2ppm) from Z-spectral fitting correlates with creatine distribution in brain tumor. NMR Biomed. 2015; 28:1–8. [PubMed: 25295758]
29. Haris M, Singh A, Cai K, et al. A technique for in vivo mapping of myocardial creatine kinase metabolism. Nat Med. 2014; 20:209–214. [PubMed: 24412924]
30. Kogan F, Haris M, Singh A, et al. Method for high-resolution imaging of creatine in vivo using chemical exchange saturation transfer. Magn Reson Med. 2014; 71:164–172. [PubMed: 23412909]
31. Kogan F, Haris M, Debrosse C, et al. In vivo chemical exchange saturation transfer imaging of creatine (CrCEST) in skeletal muscle at 3T. J Magn Reson Imaging. 2014; 40:596–602. [PubMed: 24925857]
32. Kuszewski JJ, Thottungal RA, Clore GM, et al. Automated error-tolerant macromolecular structure determination from multidimensional nuclear Overhauser enhancement spectra and chemical shift assignments: improved robustness and performance of the PASD algorithm. J Biomol NMR. 2008; 41:221–239. [PubMed: 18668206]
33. Stadlbauer A, Gruber S, Nimsky C, et al. Preoperative grading of gliomas by using metabolite quantification with high-spatial-resolution proton MR spectroscopic imaging. Radiology. 2006; 238:958–969. [PubMed: 16424238]
34. Belitzer V, Tsybakova E. About mechanism of phosphorylation, respiratory coupling. Biochimie. 1939; 4:516–533.
35. Gill SS, Thomas DG, Van Bruggen N, et al. Proton MR spectroscopy of intracranial tumours: in vivo and in vitro studies. J Comput Assist Tomogr. 1990; 14:497–504. [PubMed: 2164536]
36. Fenstermacher MJ, Narayana PA. Serial proton magnetic resonance spectroscopy of ischemic brain injury in humans. Invest Radiol. 1990; 25:1034–1039. [PubMed: 2211046]
37. Usenius JP, Vainio P, Hernesniemi J, et al. Choline-containing compounds in human astrocytomas studied by 1H NMR spectroscopy in vivo and in vitro. J Neurochem. 1994; 63:1538–1543. [PubMed: 7931308]

38. Chang L, McBride D, Miller BL, et al. Localized in vivo 1H magnetic resonance spectroscopy and in vitro analyses of heterogeneous brain tumors. J Neuroimaging. 1995; 5:157–163. [PubMed: 7626823]
39. Peeling J, Sutherland G. High-resolution 1H NMR spectroscopy studies of extracts of human cerebral neoplasms. Magn Reson Med. 1992; 24:123–136. [PubMed: 1556919]
40. Doblas S, He T, Saunders D, et al. Glioma morphology and tumor-induced vascular alterations revealed in seven rodent glioma models by in vivo magnetic resonance imaging and angiography. J Magn Reson Imaging. 2010; 32:267–275. [PubMed: 20677250]
41. Vonarbourg A, Sapin A, Lemaire L, et al. Characterization and detection of experimental rat gliomas using magnetic resonance imaging. MAGMA. 2004; 17:133–139. [PubMed: 15503254]
42. Barth RF, Kaur B. Rat brain tumor models in experimental neuro-oncology: the C6, 9L, T9, RG2, F98, BT4C, RT-2 and CNS-1 gliomas. J Neuro-Oncol. 2009; 94:299–312.
43. Recinos VR, Tyler BM, Bekelis K, et al. Combination of intracranial temozolomide with intracranial carmustine improves survival when compared with either treatment alone in a rodent glioma model. Neurosurgery. 2010; 66:530–537. discussion 537. [PubMed: 20173548]
44. Kim S, Pickup S, Hsu O, et al. Diffusion tensor MRI in rat models of invasive and well-demarcated brain tumors. NMR Biomed. 2008; 21:208–216. [PubMed: 17530617]
45. Tkac I, Starcuk Z, Choi IY, et al. In vivo 1H NMR spectroscopy of rat brain at 1 ms echo time. Magn Reson Med. 1999; 41:649–656. [PubMed: 10332839]
46. O'Gorman RL, Michels L, Edden RA, et al. In vivo detection of GABA and glutamate with MEGA-PRESS: reproducibility and gender effects. J Magn Reson Imaging. 2011; 33:1262–1267. [PubMed: 21509888]
47. Naressi A, Couturier C, Castang I, et al. Java-based graphical user interface for MRUI, a software package for quantitation of in vivo/ medical magnetic resonance spectroscopy signals. Comput Biol Med. 2001; 31:269–286. [PubMed: 11334636]
48. Naressi A, Couturier C, Devos JM, et al. Java-based graphical user interface for the MRUI quantitation package. MAGMA. 2001; 12:141–152. [PubMed: 11390270]
49. Ramani A, Dalton C, Miller DH, et al. Precise estimate of fundamental in-vivo MT parameters in human brain in clinically feasible times. Magn Reson Imaging. 2002; 20:721–731. [PubMed: 12591568]
50. Jin T, Wang P, Zong X, et al. MR imaging of the amide-proton transfer effect and the pH-insensitive nuclear overhauser effect at 9.4 T. Magn Reson Imaging. 2013; 69:760–770.
51. Zhou J. Amide proton transfer imaging of the human brain. Methods Mol Biol. 2011; 711:227–237. [PubMed: 21279604]
52. Singh A, Cai K, Haris M, et al. On B1 inhomogeneity correction of in vivo human brain glutamate chemical exchange saturation transfer contrast at 7T. Magn Reson Med. 2013; 69:818–824. [PubMed: 22511396]
53. Cai K, Xu HN, Singh A, et al. Breast cancer redox heterogeneity detectable with chemical exchange saturation transfer (CEST) MRI. Mol Imaging Biol. 2014; 16:670–679. [PubMed: 24811957]
54. Cai K, Xu HN, Singh A, et al. Characterizing prostate tumor mouse xenografts with CEST and MT-MRI and redox scanning. Adv Exp Med Biol. 2013; 765:39–45. [PubMed: 22879012]
55. Walker EA, Fenton ME, Salesky JS, et al. Magnetic resonance imaging of benign soft tissue neoplasms in adults. Radiol Clin N Am. 2011; 49:1197–1217, vi. [PubMed: 22024295]
56. Zaiss M, Xu J, Goerke S, et al. Inverse Z-spectrum analysis for spillover-, MT-, and T1-corrected steady-state pulsed CEST-MRI—application to pH-weighted MRI of acute stroke. NMR Biomed. 2014; 27:240–252. [PubMed: 24395553]
57. Patra S, Ghosh A, Roy SS, et al. A short review on creatine-creatine kinase system in relation to cancer and some experimental results on creatine as adjuvant in cancer therapy. Amino Acids. 2012; 42:2319–2330. [PubMed: 21769499]
58. Pretlow TG, Whitehurst GB, Pretlow TP, et al. Decrease in creatine kinase in human prostatic carcinoma compared to benign prostatic hyperplasia. Cancer Res. 1982; 42:4842–4848. [PubMed: 6181869]

59. Joseph J, Cardesa A, Carreras J. Creatine kinase activity and isoenzymes in lung, colon and liver carcinomas. Br J Cancer. 1997; 76:600–605. [PubMed: 9303358]
60. Tsung SH. Creatine kinase activity and isoenzyme pattern in various normal tissues and neoplasms. Clin Chem. 1983; 29:2040–2043. [PubMed: 6640897]
61. Onda T, Uzawa K, Endo Y, et al. Ubiquitous mitochondrial creatine kinase downregulated in oral squamous cell carcinoma. Br J Cancer. 2006; 94:698–709. [PubMed: 16479256]
62. Patra S, Bera S, SinhaRoy S, et al. Progressive decrease of phosphocreatine, creatine and creatine kinase in skeletal muscle upon transformation to sarcoma. FEBS J. 2008; 275:3236–3247. [PubMed: 18485002]
63. Fukuda J, Yagishita S, Yamaoka K, et al. Creatine kinase isoenzyme BB increased in serum and tumor tissue of patients with giant cell tumor of bone. Clin Chem. 1994; 40:2064–2065. [PubMed: 7955379]
64. Meffert G, Gellerich FN, Margreiter R, et al. Elevated creatine kinase activity in primary hepatocellular carcinoma. Boston Med Ctr Gastroenterol. 2005; 5:9.
65. Tain RLW, Yang S, Zhou XJ, et al. Separated quantification of creatine and phosphocreatine based on a novel proton MR method combing 1H-MRS and CEST MRI. Process Intl Soc Magn Reson Med. 2015; 23:3352.
66. Mori S, Eleff SM, Pilatus U, et al. Proton NMR spectroscopy of solvent-saturable resonances: a new approach to study pH effects in situ. Magn Reson Med. 1998; 40:36–42. [PubMed: 9660550]
67. Jin T, Wang P, Zong X, et al. Magnetic resonance imaging of the Amine-Proton EXchange (APEX) dependent contrast. Neuroimage. 2012; 59:1218–1227. [PubMed: 21871570]
68. Desmond KL, Moosvi F, Stanisz GJ. Mapping of amide, amine, and aliphatic peaks in the CEST spectra of murine xenografts at 7 T. Magn Reson Med. 2014; 71:1841–1853. [PubMed: 23801344]
69. Sun PZ, Benner T, Kumar A, et al. Investigation of optimizing and translating pH-sensitive pulsed-chemical exchange saturation transfer (CEST) imaging to a 3T clinical scanner. Magn Reson Med. 2008; 60:834–841. [PubMed: 18816867]
70. Arus C, Barany M, Westler WM, et al. 1H NMR of intact muscle at 11 T. FEBS Lett. 1984; 165:231–237. [PubMed: 6607178]
71. Middleton DA, Hockings PD, Glen S, et al. Image directed proton spectroscopy of gerbil brain at 7 tesla. NMR Biomed. 1995; 8:118–126. [PubMed: 8579999]
72. Wu LM, Zhou B, Lu Q, et al. T2* relaxation time in the detection and assessment of aggressiveness of peripheral zone cancer in comparison with diffusion-weighted imaging. Clin Radiol. 2016; 71:356–362. [PubMed: 26823021]
73. Simpkin CJ, Morgan VA, Giles SL, et al. Relationship between T2 relaxation and apparent diffusion coefficient in malignant and nonmalignant prostate regions and the effect of peripheral zone fractional volume. Br J Radiol. 2013; 86:20120469. [PubMed: 23426849]
74. Just M, Thelen M. Tissue characterization with T1, T2, and proton density values: results in 160 patients with brain tumors. Radiology. 1988; 169:779–785. [PubMed: 3187000]
75. Felix R, Schorner W, Laniado M, et al. Brain tumors: MR imaging with gadolinium-DTPA. Radiology. 1985; 156:681–688. [PubMed: 4040643]
76. Aronen HJ, Gazit IE, Louis DN, et al. Cerebral blood volume maps of gliomas: comparison with tumor grade and histologic findings. Radiology. 1994; 191:41–51. [PubMed: 8134596]
77. Shin JH, Lee HK, Kwun BD, et al. Using relative cerebral blood flow and volume to evaluate the histopathologic grade of cerebral gliomas: preliminary results. Am J Roentgenol. 2002; 179:783–789. [PubMed: 12185064]
78. Arnold DL, Shoubridge EA, Villemure JG, et al. Proton and phosphorus magnetic resonance spectroscopy of human astrocytomas in vivo. Preliminary observations on tumor grading. NMR Biomed. 1990; 3:184–189. [PubMed: 2169842]
79. Bruhn H, Frahm J, Gyngell ML, et al. Noninvasive differentiation of tumors with use of localized H-1 MR spectroscopy in vivo: initial experience in patients with cerebral tumors. Radiology. 1989; 172:541–548. [PubMed: 2748837]
80. Law M, Yang S, Wang H, et al. Glioma grading: sensitivity, specificity, and predictive values of perfusion MR imaging and proton MR spectroscopic imaging compared with conventional MR imaging. Am J Neuroradiol. 2003; 24:1989–1998. [PubMed: 14625221]

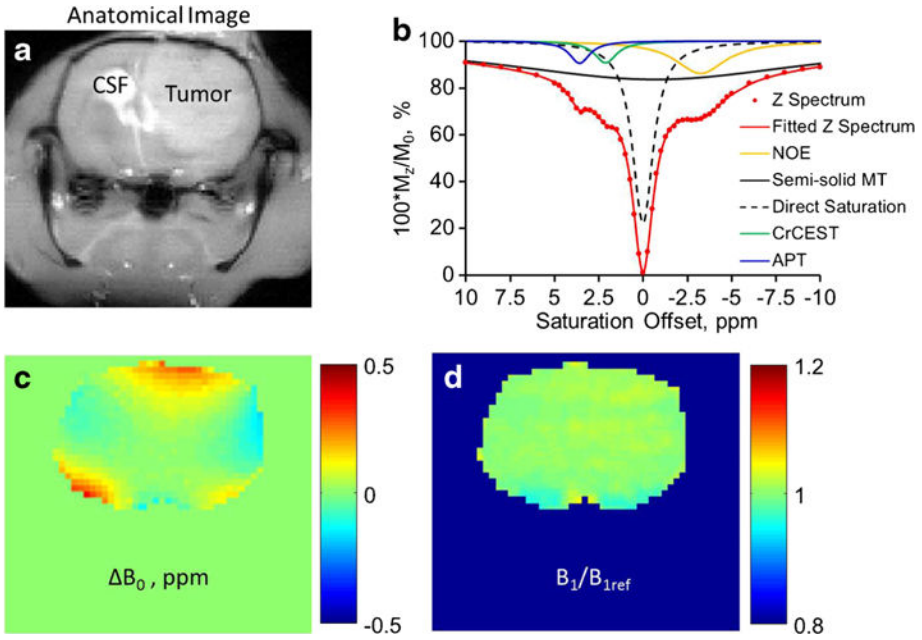

Fig. 1.

a Anatomical tumor-bearing images of the rat brain acquired at −2 ppm pre-saturation with tumor and cerebrospinal fluid (CSF) regions indicated. **b** Demonstration of the multicomponent fitting of an experimental tumor Z-spectrum for the separated quantification of NOE, semi-solid MTC, direct saturation, CrCEST, and APT. **c** B_0 map of the brain. **d** B_1 map or B_1 to reference B_1 ratio (B_1/B_{1ref}) map of the brain.

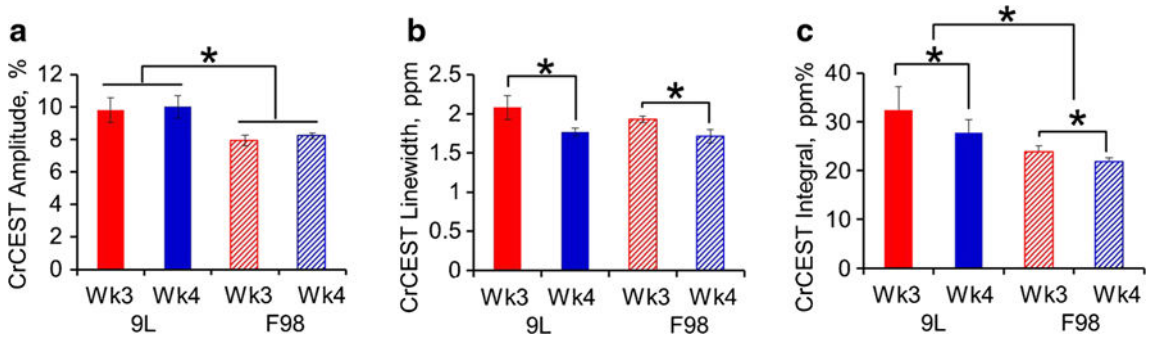

Fig. 2.

The **a** amplitude, **b** linewidth, and **c** integral of the fitted CrCEST peak from 9L and F98 gliomas at weeks 3 ($n = 5$) and 4 ($n = 4$) post-tumor implantation. *$p < 0.05$.

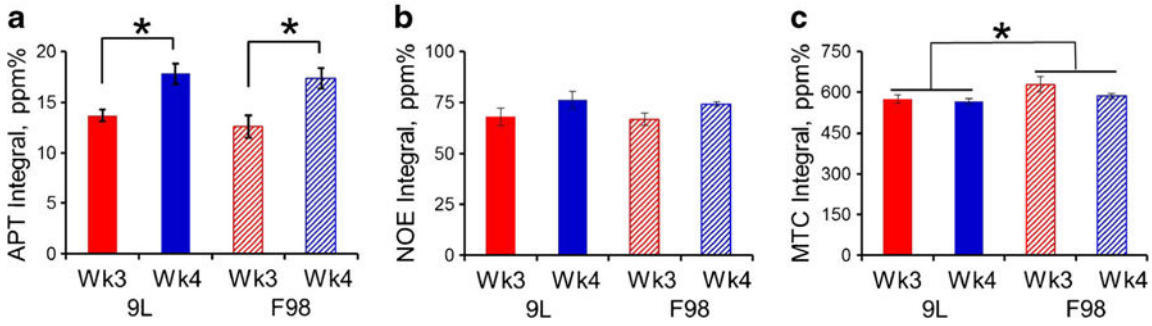

Fig. 3.

The integral of the fitted **a** APT, **b** NOE, and **c** MTC peaks from 9L and F98 gliomas at weeks 3 ($n = 5$) and 4 ($n = 4$) post-tumor implantation. *$p < 0.05$.

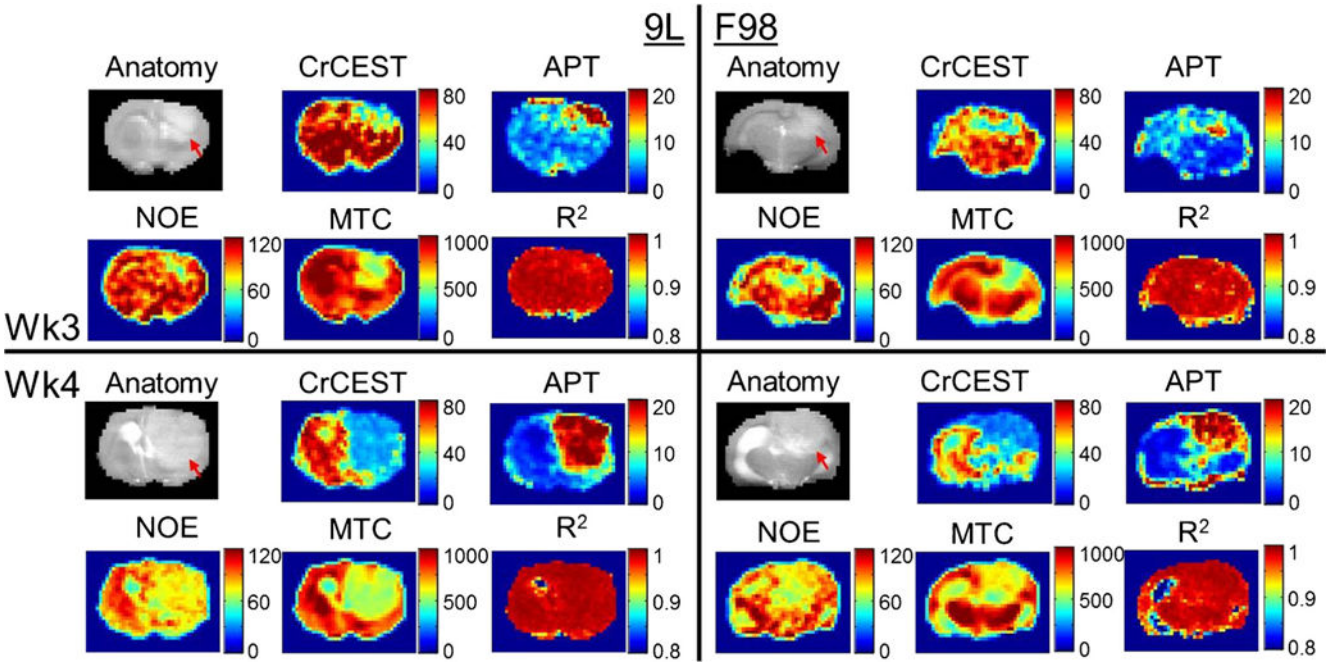

Fig. 4.

Anatomical tumor-bearing images of the brain acquired with saturation at −2 ppm (*gray scaled, red arrows* indicate tumors), the corresponding *CrCEST, APT, NOE*, and *MTC* integral maps (*false colored*), and fitting R^2 maps from 9L (*left panels*) and F98 (*right panels*) brain tumors at the third (*top panels*) or fourth (*bottom* panels) week post-tumor implantation.

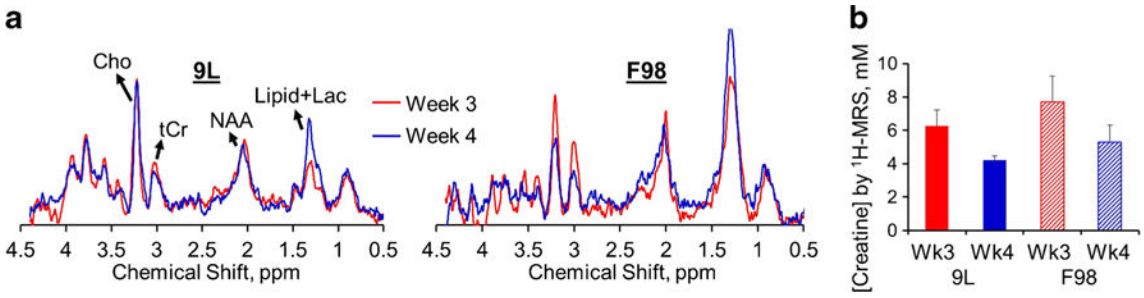

Fig. 5.

a Normalized with the corresponding water reference signals, MR spectra from 9L and F98 tumors were averaged at week 3 ($n = 5$ for 9L, reduced $n = 3$ for F98 due to MRS quality issues) and week 4 ($n = 4$ for both 9L and F98) post-tumor implantation. **b** Creatine concentrations quantified from ^{1}H-MRS is shown. *Cho* choline, *Cr* creatine, *NAA N*-acetylaspartic acid, *Lac* lactate.